Discovery of excess O I absorption towards the $z = 6.42$ QSO SDSS J1148+5251[1]

George D. Becker[2], Wallace L. W. Sargent[2], Michael Rauch[3], Robert A. Simcoe[4]

ABSTRACT

We present a search for O I in the spectra of nine $4.9 \leq z_{\mathrm{QSO}} \leq 6.4$ QSOs taken with Keck/HIRES. We detect six systems with $N_{\mathrm{O\,I}} > 10^{13.7}$ cm^{-2} in the redshift intervals where O I $\lambda 1302$ falls redward of the Lyα forest. Four of these lie towards SDSS J1148+5251 ($z_{\mathrm{QSO}} = 6.42$). This imbalance is unlikely to arise from variations in sensitivity among our data or from a statistical fluctuation. The excess O I occurs over a redshift interval that also contains transmission in Lyα and Lyβ. Therefore, if these O I systems represent pockets of neutral gas, then they must occur within or near regions of the IGM that are highly ionized. In contrast, no O I is detected towards SDSS J1030+0524 ($z_{\mathrm{QSO}} = 6.30$), whose spectrum shows complete absorption in Lyα and Lyβ over $\Delta z \sim 0.2$. Assuming no ionization corrections, we measure mean abundance ratios $\langle [\mathrm{O/Si}] \rangle = -0.04 \pm 0.06$, $\langle [\mathrm{C/O}] \rangle = -0.31 \pm 0.09$, and $\langle [\mathrm{C/Si}] \rangle = -0.34 \pm 0.07$ (2σ), which are consistent with enrichment dominated by Type II supernovae. The O/Si ratio limits the fraction of silicon in these systems contributed by metal-free very massive stars to $\lesssim 30\%$, a result which is insensitive to ionization corrections. The ionic comoving mass densities along the $z_{\mathrm{QSO}} > 6.2$ sightlines, including only the detected systems, are $\Omega_{\mathrm{O\,I}} = (7.0 \pm 0.6) \times 10^{-8}$, $\Omega_{\mathrm{Si\,II}} = (9.6 \pm 0.9) \times 10^{-9}$, and $\Omega_{\mathrm{C\,II}} = (1.5 \pm 0.2) \times 10^{-8}$.

Subject headings: cosmology: observations — cosmology: early universe — intergalactic medium — quasars: absorption lines — quasars: individual (SDSS J2225-0014, SDSS J1204-0021 SDSS J0915+4244, SDSS J0231-0728, SDSS J0836+0054, SDSS J0002+2550, SDSS J1623+3112, SDSS J1030+0524, SDSS J1148+5251)

---

[1]The observations were made at the W.M. Keck Observatory which is operated as a scientific partnership between the California Institute of Technology and the University of California; it was made possible by the generous support of the W.M. Keck Foundation.

[2]Palomar Observatory, California Institute of Technology, Pasadena, CA 91125, USA; gdb@astro.caltech.edu, wws@astro.caltech.edu

[3]Carnegie Observatories, 813 Santa Barbara Street, Pasadena, CA 91101, USA; mr@ociw.edu

[4]MIT Center for Space Research, 77 Massachusetts Ave. #37-664B, Cambridge, MA 02139, USA; simcoe@mit.edu

1. Introduction

The state of the intergalactic medium (IGM) at redshift $z \sim 6$ remains under considerable debate. Significant transmitted flux in the Lyα forest at $z \sim 5.7$ means that the IGM must have been highly ionized by at least ~ 1 Gyr after the Big Bang (Becker et al. 2001; Djorgovski et al. 2001; Fan et al. 2001, 2004). Each of the four known QSOs at $z_{\rm QSO} \geq 6.2$ show Gunn-Peterson troughs (Gunn & Peterson 1965) over at least a narrow redshift interval (Becker et al. 2001; Pentericci et al. 2002; Fan et al. 2001, 2003, 2004; White et al. 2003). This complete lack of transmitted flux has been interpreted as an indication that the tail end of cosmic reionization may extend to $z \sim 6$. However, Songaila (2004) found the evolution of transmitted flux over $2 < z < 6.3$ to be consistent with a smoothly decreasing ionization rate and not indicative of a sudden jump in the Lyα optical depth at $z \sim 6$.

Significant variations in the fraction of transmitted flux are common among sightlines at the same redshift (Songaila 2004). While the spectrum of SDSS J1030+0524 ($z_{\rm QSO} = 6.30$) shows complete absorption in Lyα and Lyβ over a redshift interval $\Delta z \approx 0.2$ (White et al. 2003), transmitted flux appears over the same redshifts in the Lyα, Lyβ, and Lyγ forests of SDSS J1148+5251 ($z_{\rm QSO} = 6.42$) (White et al. 2005; Oh & Furlanetto 2005). Either the IGM is highly ionized everywhere at $z \sim 6.3$ and long stretches of complete absorption are the result of line blending, or the neutral fraction of the IGM is patchy on large scales. A patchy IGM could result from the clumpiness of the IGM and the clustering of ionizing sources (Furlanetto & Oh 2005).

Studies of H I transmitted flux are ultimately hampered by the large optical depths expected for even a small neutral fraction. The presence of a Gunn-Peterson trough can at best constrain the volume- and mass-weighted H I neutral fractions to $\gtrsim 10^{-3}$ and $\gtrsim 10^{-2}$, respectively (Fan et al. 2002). Alternative measurements are required to probe larger neutral fractions. The non-evolution in the luminosity function of Lyα-emitting galaxies provides an independent indication that the IGM at $z \sim 6.5$ is highly ionized (e.g., Malhotra & Rhoads 2004; Stern et al. 2005), although Lyα photons may escape as a result of galactic winds (Santos 2004) or from locally ionized bubbles created by clustered sources (Furlanetto et al. 2004a). In the future, observations of redshifted 21 cm emission/absorption should trace the growth and evolution of ionized regions at $z > 6$, placing strong constraints on reionization scenarios (e.g., Tozzi et al. 2000; Kassim et al. 2004; Carilli et al. 2004; Furlanetto et al. 2004b).

A high neutral fraction must also have a measurable effect on metal absorption lines (Oh 2002; Furlanetto & Loeb 2003). Overdense regions of the IGM should be the first to become enriched, due to the presence of star-forming sources, yet the last to remain ionized, due to the short recombination times (Oh 2002). Low-ionization metal species should therefore produce

numerous absorption features in the spectra of background objects prior to reionization. A particularly good candidate is O I, which has an ionization potential nearly identical to that of H I and a transition at 1302 Å that can be observed redward of the Lyα forest. Oxygen and hydrogen will lock in charge-exchange equilibrium (Osterbrock 1989), which ensures that their neutral fractions will remain nearly equal,

$$f_{\mathrm{H\,I}} \equiv \frac{n_{\mathrm{H\,I}}}{n_{\mathrm{H}}} \approx \frac{n_{\mathrm{O\,I}}}{n_{\mathrm{O}}} \,. \tag{1}$$

Despite the increased photo-ionization cross section of O I at higher energies, this relationship is expected to hold over a wide range in $f_{\mathrm{H\,I}}$ (Oh et al. 2005, in prep).

In this work, we present a search for O I in the spectra of nine $4.9 \leq z_{\mathrm{QSO}} \leq 6.4$ QSOs. This is the first time a set of $z_{\mathrm{QSO}} > 5$ spectra has been taken at high resolution (R = 45,000). Our sample includes three objects at $z_{\mathrm{QSO}} > 6.2$, where we might expect to see an "O I forest" (Oh 2002). In §2 we describe the observations and data reduction. The results of the O I search are detailed in §3. In §4 we demonstrate a significant overabundance of O I systems towards the highest-redshift object, SDSS J1148+5251 ($z_{\mathrm{QSO}} = 6.42$), and compare the overabundance to the number density of lower-redshift O I systems and other absorbers with high H I column densities. Measurements of the relative metal abundances for all the detected systems are described in §5. In §6 we discuss the significance of these excess systems for the enrichment and ionization state of the IGM at $z \sim 6$. Our results are summarized in §7. Throughout this paper we assume $\Omega = 1$, $\Omega_{\mathrm{m}} = 0.3$, $\Omega_{\Lambda} = 0.7$, and $H_0 = 70$ km s^{-1} Mpc^{-1}.

2. The Data

Observations using the Keck HIRES spectrograph (Vogt et al. 1994) were made between 2003 February and 2005 June, with the bulk of the data acquired during 2005 January and February. Our QSO sample and the observations are summarized in Table 1. All except the 2003 February data were taken with the upgraded HIRES detector. We used an $0.''86$ slit, which gives a velocity resolution FWHM of $\Delta v = 6.7$ km s^{-1}.

The continuum luminosities in our sample approach the practical detection limit of HIRES. In addition, the spectral regions of interest for this work lie in the far red, where skyline contamination and atmospheric absorption are major concerns. To address these difficulties, the data were reduced using a custom set of IDL routines written by one of us (GDB). This package uses optimal sky subtraction (Kelson 2003) to achieve Poisson-limited residuals in the two-dimensional sky-subtracted frame. One-dimensional spectra were extracted using optimal extraction (Horne 1986). Blueward of the Lyα emission line,

the continuum for these objects is highly obscured due to strong absorption from the Lyα forest. Furthermore, single exposures were typically too faint to fit reliable continua even in unabsorbed regions. Individual orders were therefore combined by first flux calibrating each order using the response function derived from a standard star. The combined spectra were continuum-fit by hand using a cubic spline. Standards stars were also to correct for telluric absorption. Estimated residuals from continuum fitting (redward of Lyα) and atmospheric correction are typically within the flux uncertainties.

3. O I Search

3.1. Technique

At $z > 5$ it becomes increasingly difficult to identify individual Lyα lines due to the large opacity in the Lyα forest. Therefore, candidate O I lines must be confirmed using other ions at the same redshift. Si II $\lambda1260$ and C II $\lambda1334$ are the most useful for this purpose since their rest wavelengths place them redward of the Lyα forest, at least over a limited range in redshift. These transitions are also expected to be relatively strong over a range in ionization conditions. At lower redshifts where Si II $\lambda1260$ has entered the forest, we are still sensitive to Si II $\lambda1304$, although it is weaker than Si II $\lambda1260$ by a factor of 7.

We searched for O I in each sightline over the redshift range between the quasar redshift $z_{\rm QSO}$ and the redshift $z_{\rm min} = (1 + z_{\rm QSO})\lambda_\alpha/\lambda_{\rm O\,I} - 1$, where O I enters the Lyα forest. To identify a system, we required absorption at the same redshift in O I and either Si II $\lambda1260$ or C II $\lambda1334$, and that the line profiles for at least two of the ions be comparable. In practice, Si II $\lambda1260$ proved to be the best indicator over the lower-redshift end of each sightline, since the signal-to-noise (S/N) ratio was typically better over that region of the spectrum. At redshifts where Si II $\lambda1260$ was lost in the forest we relied solely upon C II for confirmation. By chance, the two O I systems we identified using only C II were also strong enough to be detected in Si II $\lambda1304$.

We identified six O I systems in total along our nine lines of sight. Their properties are summarized in Table 2. Four of the six systems appear towards SDSS J1148+5251, and we examine this potential overabundance in detail in §4. Voigt profiles were fitted using the VPFIT package written, by R. Carswell. Due to line blending and the modest S/N ratio over some regions of the data, it was often necessary to tie the redshift and/or Doppler parameter of one ion to those of another whose profile was more clearly defined in order to obtain a satisfactory fit. In practice, the resulting total column densities are very similar to those obtained when all parameters are allowed to vary freely, as would be expected for

systems still on the linear part of the curve of growth. Comments on individual systems are given below.

3.1.1. SDSS J0231−0728: $z_{\rm sys} = 5.3364$ (Figure 1)

This system shows a central complex in O I, Si II, and C II that is best fit using three components with a total velocity span of $\Delta v \approx 38$ km s^{-1}. We measure the redshifts and b-parameters of the bluest two central components from Si II. The redshift and b-parameter for the reddest central component are measured from O I, which is least affected by additional lines towards the red. Leaving all parameters untied produces a two-component fit for C II, which is likely due to low S/N. However, the total column densities remain virtually unchanged.

A single component at $\Delta v \approx -115$ km s^{-1} appears in Si II and C II but not in O I. Since O I is more easily ionized than either Si II or C II ($\Delta E_{\rm O\,I} = 13.6$ eV, $\Delta E_{\rm Si\,II} = 16.3$ eV, $\Delta E_{\rm C\,II} = 24.4$ eV) this component probably arises from gas that is more highly ionized than the gas producing the O I absorption. Three additional components appear redward of the central O I complex. These are visible in Si II, C II, and Si IV and presumably correspond to gas in a still higher ionization state. We use Si II to constrain the redshift and b-parameters for all the non-O I components, although fitting without tying any parameters produces very similar results.

3.1.2. SDSS J1623+3112: $z_{\rm sys} = 5.8408$ (Figure 2)

This system shows multiple components with a total velocity span of $\Delta v \approx 81$ km s^{-1}. The Si II is strong enough that the 1304 Å transition is clearly visible. Some additional absorption occurs along the blue edge of the O I complex. However, since no corresponding absorption appears in C II this features is unlikely to be genuine O I. We use C II to fix the redshifts and b-parameters of the bluest two components and the reddest component for all ions. The z and b values for the remaining components are tied to O I. The weakest C II component was automatically dropped by the fitting program. However, this should not have a significant impact on the summed C II column density. No Si IV was detected down to $N_{\rm Si\,IV} > 10^{13}$ cm^{-2}.

A strong line appears at a velocity separation $\Delta v \approx -180$ km s^{-1} from the O I complex. Weak absorption appears at the same velocity in Si II λ1304. However, the corresponding C II region is completely covered by Mg I λ2853 from a strong Mg II system at $z_{\rm abs} = 2.1979$.

Therefore, while these features are plausibly associated with the O I complex, their identity cannot presently be confirmed. We do not include these lines when computing the relative abundances, although their O I/Si II ratio is consistent with those measured for the other O I systems.

3.1.3.   SDSS J1148+5251: $z_{\mathrm{sys}} = 6.0097$ (Figure 3)

This system shows multiple components with a velocity span of $\Delta v \approx 41$ km s^{-1}. The Si II $\lambda 1260$ transition falls in the Lyα forest. However, Si II $\lambda 1304$ is clearly visible. The C II occurs among moderate-strength telluric absorption. In correcting for the atmosphere we recovered a C II velocity profile very similar to that of O I and Si II. Some additional absorption around the C II are probably telluric lines that were not completely removed. We achieved the best fit for O I using four components while allowing the continuum level to vary slightly. Using fewer components resulted in virtually the same total $N_{\mathrm{O\,I}}$, which is to be expected if the lines lie along the linear part of the curve of growth. We used the z and b values for these four O I lines to determine the corresponding column densities for Si II and C II. Leaving all parameters untied resulted in small changes in the b-parameters and in the preferred number of lines used by VPFIT (3 for Si II instead of 4), but negligible changes in the total column density for each ion. We detect no Si IV down to $N_{\mathrm{Si\,IV}} > 10^{12.5}$ cm^{-2}. This system does show C IV absorption in the low-resolution NIRSPEC spectrum taken by Barth et al. (2003). However, the kinematic structure cannot be determined from their data, and it is therefore unknown whether the C IV absorption arises from the same gas that produces the lower-ionization lines.

3.1.4.   SDSS J1148+5251: $z_{\mathrm{sys}} = 6.1293$ (Figure 4)

The Si II $\lambda 1260$ line for this system falls in the Lyα forest. However, Si II $\lambda 1304$ is strong enough to be visible. We tie the redshifts and b-parameters for Si II and C II at $z = 6.129267$ to those for O I, which has the cleanest profile. Leaving all parameters untied produces changes in the b-parameters that are within the errors and negligible changes in the column densities. Possible additional C II lines appear at $\Delta v = -67$, -29, and 26 km s^{-1} from the strong component. These do not appear in O I and would probably be too weak to appear in Si II $\lambda 1304$. We do not include them when computing the relative abundances for this system. No Si IV was detected down to $N_{\mathrm{Si\,IV}} > 10^{12.7}$ cm^{-2}.

3.1.5. SDSS J1148+5251: $z_{\mathrm{sys}} = 6.1968$ (Figure 5)

The Si II λ1260 and C II lines for this system occur in transparent gaps within regions of mild telluric absorption. In some of our exposures, the O I line falls on the blue wing of a strong telluric feature. However, the O I can be clearly seen in the uncorrected 2005 January data, where the heliocentric velocity shifted the observed QSO spectrum further to the blue. We tie the redshifts and b-values for O I and C II to those of Si II, for which the line profile is the cleanest. Leaving all parameters untied produces negligible changes in the column densities.

3.1.6. SDSS J1148+5251: $z_{\mathrm{sys}} = 6.2555$ (Figure 6)

We use a single component for the primary fit to this system. The C II falls on a sky emission line and hence the line profile is rather noisy. We therefore tied the redshift and b-parameter for C II to those of Si II, while z and b for O I were allowed to vary freely. The fitted z and b values for O I agree with those for Si II within the fit errors. Tying z and b for O I to those of Si II produced no significant change in $N_{\mathrm{O\,I}}$. Both Si II λ1260 and O I are well fit by a single line, while the blue edge of the C II shows a possible additional component. We fit this component separately but do include it when computing relative abundances.

4. Overabundance of O I systems towards SDSS J1148+5251

Despite the relatively small total number of detected O I systems, a noticable overabundance appears towards SDSS J1148+5251. It should be noted that this object has one of the brightest continuum magnitudes among QSOs at $z > 5$ (Fan et al. 2003). We also spent considerable integration time on this object. Therefore, the data are among the best in our sample. In this section we address the null hypothesis that the apparent imbalance in the distribution of O I systems results from a combination of incompleteness and small number statistics.

For each sightline we used an automated scheme to determine the absorption pathlength interval ΔX over which we are sensitive to systems above a given O I column density. For a non-evolving population of sources expanding with the Hubble flow, we expect to intersect the same number of sources per unit X at all redshifts, where X is defined for $\Omega = 1$ as

$$dX = \frac{(1+z)^2}{\sqrt{\Omega_{\mathrm{m}}(1+z)^3 + \Omega_\Lambda}} dz \, . \tag{2}$$

At the redshift of each pixel where we are potentially sensitive to O I, we inserted artificial single-component systems containing O I, Si II, and C II with relative abundances set to the mean measured values (see §5) and a turbulent Doppler width of $b = 10$ km s^{-1}. The minimum $N_{\rm O\,I}$ at which the system could be detected by the automated program was then determined. A detection required that there be significant (4σ) absorption at the expected wavelengths of O I and at least one of the other two ions. The redshifts of at least two of the three fitted profiles must also agree within a tolerance of $\Delta z_{tol} = 0.0002$, and the line widths must agree to within a factor of two. In the case where the fitted profiles agree for only two of the ions, the spectrum at the wavelength of the third ion must be consistent with the expected level of absorption. This allows for one of the ions to be blended with another line or lost in Lyα forest. Lines that fell in the Fraunhofer A band were not considered. This method detected all of the known O I systems and produced only one false detection in the real data, which was easily dismissed by visual inspection. We note that this method focuses on our ability to detect systems similar to those observed towards SDSS J1148+5251. Multiple-component systems such as the two at lower redshift are in general easy to identify, even in noisy regions of the spectrum.

The results of the sensitivity measurements are shown in Figure 9. The solid lines show the ΔX over which we are sensitive to systems with $N_{\rm O\,I} \geq N_{\rm O\,I}^{\rm min}$. The O I column densities for the four systems seen towards SDSS J1148+5251 are marked with circles. The dashed line shows the mean ΔX as a function of $N_{\rm O\,I}^{\rm min}$ for all nine sightlines. While it is clear that the path length over which we are sensitive to low-column density systems is considerably smaller for some sightlines than for SDSS J1148+5251, there does exist significant coverage across the total sample even at the $N_{\rm O\,I}$ of the weakest system in our sample.

Completeness effects will depend on the intrinsic distribution of line strengths, in that weaker systems will more easily be lost in low-S/N sightlines. It is useful to define an effective absorption pathlength interval $\Delta X^{\rm eff}$ such that, for a sightline with a total pathlength $\Delta X^{\rm tot}$ and sensitivity $S(N)$, we would expect to detect the same number $\mathcal{N}$ of systems with $N \geq N_{\rm min}$ over $\Delta X^{\rm eff}$ if we had perfect sensitivity. For a column-density distribution $f(N) = \partial^2 \mathcal{N}/\partial N \partial X$, this gives

$$\Delta X^{\rm eff} \int_{N_{\rm min}}^{\infty} f(N)\, dN = \Delta X^{\rm tot} \int_{N_{\rm min}}^{\infty} f(N)\, S(N)\, dN\,, \tag{3}$$

where $S(N)$ is the fraction of the total pathlength over which we are sensitive to systems with column density N. The sensitivity function can be determined directly from Figure 9. We assume a conventional power-law distribution in O I column densities $f(N_{\rm O\,I}) \propto N_{\rm O\,I}^{-\alpha}$. Hence,

$$\Delta X^{\rm eff} = \Delta X^{\rm tot} \frac{\int_{N_{\rm min}}^{\infty} N^{-\alpha}\, S(N)\, dN}{\int_{N_{\rm min}}^{\infty} N^{-\alpha}\, dN}\,. \tag{4}$$

Taking into account our measured sensitivity, the maximum likelihood estimator for α for all six O I systems is $\hat{\alpha} = 1.7$. A K-S test allows $1.3 \leq \alpha \leq 2.1$ at the 95% confidence level.

In Figure 10 we plot ΔX^{eff} as a function of α taking $N_{\mathrm{min}} = 10^{13.7}$ cm^{-2} as the cutoff value. The solid line shows ΔX^{eff} for SDSS J1148+5251, while the dashed line shows ΔX^{eff} for the remaining eight sightlines, divided by 5.7 to match SDSS J1148+5251 at $\alpha = 1.7$. It is easy to see that the ratio $\Delta X^{\mathrm{eff}}_{1148}/\Delta X^{\mathrm{eff}}_{\mathrm{other}}$ does not change significantly with α ($\lesssim 4\%$ over $1.1 \leq \alpha \leq 3.0$). This is purely a coincidence, most likely related to the fact that the overall high quality of the SDSS J1148+5251 data is balanced by the placement of the O I systems in a difficult region of the spectrum. However, it means that the relative numbers of expected O I detections for SDSS J1148+5251 and the remaining eight sightlines should be nearly invariant over a wide range in plausible column density distributions.

We can now evaluate the likelihood that the imbalance of O I detection results from small number sampling. For a Poisson distribution, the likelihood of detecting $\mathcal{N}$ systems when the expected number of detections is ν is given by

$$P(\mathcal{N}, \nu) = \frac{\nu^{\mathcal{N}} e^{-\nu}}{\mathcal{N}} \,. \tag{5}$$

If we assume that the expected number of detections towards SDSS J1148+5251 is $\nu = 6 \left(\Delta X^{\mathrm{eff}}_{1148}/\Delta X^{\mathrm{eff}}_{\mathrm{all}} \right) \simeq 0.90$, then the probability of detecting at least 4 systems is

$$P(\geq 4, \nu) = \sum_{\mathcal{N}=4}^{\infty} P(\mathcal{N}, \nu) = 1 - \sum_{\mathcal{N}=0}^{3} P(\mathcal{N}, \nu) = 0.013 \,. \tag{6}$$

Similarly, if we take the number of systems observed towards SDSS J1148+5251 as a representative sample and compute the expected number of systems towards the remaining eight sightlines to be $\nu = 4 \left(\Delta X^{\mathrm{eff}}_{\mathrm{other}}/\Delta X^{\mathrm{eff}}_{1148} \right) \simeq 23$, then the likelihood of detecting at most two systems is

$$P(\leq 2, \nu) = \sum_{\mathcal{N}=0}^{2} P(\mathcal{N}, \nu) = 3.6 \times 10^{-8} \,. \tag{7}$$

The probability of simultaneously detecting at least 4 systems towards SDSS J1148+5251 while detecting at most two systems along the remaining eight sightlines,

$$P\left(\frac{\partial \mathcal{N}}{\partial X} \right) = \left[1 - \sum_{\mathcal{N}=0}^{3} P(\mathcal{N}, \frac{\partial \mathcal{N}}{\partial X} \Delta X^{\mathrm{eff}}_{1148}) \right] \left[\sum_{\mathcal{N}=0}^{2} P(\mathcal{N}, \frac{\partial \mathcal{N}}{\partial X} \Delta X^{\mathrm{eff}}_{\mathrm{other}}) \right] \,, \tag{8}$$

has a maximum of $P(\partial \mathcal{N}/\partial X) = 0.0018$ at $\partial \mathcal{N}/\partial X = 0.84$, taking $\alpha \leq 3$. Thus, assuming that the O I systems are randomly distributed, we can rule out with a high degree of confidence the possibility that the excess number of detected systems towards SDSS J1148+5251 is the result of a statistical fluctuation.

4.1. Comparison with Lower-Redshift Sightlines

Our sample of nine $z_{\rm QSO} > 4.8$ sightlines is sufficient to demonstrate that the apparent excess of O I systems towards SDSS 1148+5251 is highly unlikely to arise from a random spatial distribution of absorbers. However, the distribution may be significantly non-random due to large-scale clustering. For example, if the line-of-sight towards SDSS 1148+5251 passes through an overdense region of the IGM then we might expect to intersect more than the typical number of absorbers.

To address this possibility, we have searched for O I in the spectra of an additional 30 QSOs with $2.6 < z_{\rm QSO} < 4.6$. The sample was taken entirely with HIRES for a variety of studies. Due to the lower QSO redshifts, the data are of significantly higher quality than the $z_{\rm QSO} > 4.8$ sample. All sightlines are complete down to $N_{\rm O\,I} = 10^{13.5}$ cm^{-2} (apart from rare wavelength coverage gaps) with the majority complete down to $N_{\rm O\,I} = 10^{13.0}$ cm^{-2}.

A detailed study of the properties of lower-redshift O I absorbers will be presented elsewhere. Here we note that 11 systems with $N_{\rm O\,I} > 10^{13.7}$ cm^{-2} were identified along all 30 sightlines in the redshift intervals where O I would occur redward of the Lyα forest. This is comparable to but slightly larger than the incidence rate among the eight lowest-redshift sightlines in our $z_{\rm QSO} > 4.8$ sample. The number density is even somewhat higher among the $z_{\rm QSO} < 4.6$ sample since the absorption pathlength intervals are shorter (cf. Eq. 2). However, many of the $z_{\rm QSO} < 4.6$ spectra were taken in order to study known damped Lyα systems (DLAs; $N_{\rm H\,I} > 10^{20.3}$ cm^{-2}), which commonly exhibit O I (e.g., Prochaska et al. 2001, 2003). We would therefore expect these sightlines to contain more than the typical number of O I systems. The important point is that no sightline contained more than a single system. If the excess towards SDSS J1148+5251 is due to the chance alignment with an overdense region of the IGM, then such a coincidence must occur in fewer than $\sim 2 - 3\%$ of all sightlines.

4.2. Comparison with Damped Lyα and Lyman Limit System Populations

We can compare the observed number of O I systems in our $z_{\rm QSO} > 4.8$ sample with the expected number of DLAs by extrapolating from lower-redshift DLA surveys. Storrie-Lombardi & Wolfe (2000) find a line number density $n_{\rm DLA}(z) = \partial \mathcal{N}_{\rm DLA}/\partial z = 0.055\,(1+z)^{1.11}$. This is consistent at high-z with the larger survey done by Prochaska et al. (2005) and with the number density evolution Rao et al. (2005) obtained by combining DLA samples over $0 \leq z \leq 4.5$. From this $n_{\rm DLA}(z)$ we would expect a total of ~ 1.5 DLAs total along all nine lines-of-sight in the redshift intervals where are sensitive to O I. This is consistent with the

two O I systems seen along the eight lower-redshift sightlines. However, we would expect to see only ~ 0.2 DLAs towards SDSS J1148+5251, which is inconsistent with the four we observe.

The disparity eases for SDSS J1148+5251 if we include all Lyman limit Systems (LLSs; $N_{\rm H\,I} > 10^{17.2}$ cm^{-2}). The line number density of LLSs at $z > 2.4$ found by Péroux et al. (2003), $n_{\rm LLS}(z) = 0.07\,(1+z)^{2.45}$, predicts ~ 4 LLSs towards SDSS J1148+5251 in the interval where we can observe O I. However, there should also be ~ 20 LLSs along the remaining eight lines-of-sight. If the excess O I absorbers are associated with the progenitors of lower-redshift LLSs then they must evolve strongly in O I at $z \gtrsim 6$.

5. Metal Abundances

Absorption systems at $z > 5$ provide an opportunity to study metal enrichment when the age of the Universe was $\lesssim 1$ Gyr. The opacity of the Lyα forest at these redshifts prevents us from measuring reliable H I column densities. However, we are still able to constrain relative abundances. In Table 3 we summarize the Voigt profile fitting results. Total column densities for each system include only components with confirmed O I. Relative abundances were calculated using the solar values of Grevesse & Sauval (1998) and assuming zero ionization corrections. These are plotted in Figure 11. The error-weighted mean values for all six systems are $\langle[\rm O/Si]\rangle = -0.04 \pm 0.06$, $\langle[\rm C/O]\rangle = -0.31 \pm 0.09$, and $\langle[\rm C/Si]\rangle = -0.34 \pm 0.07$ (2σ errors).

The uncorrected abundances are broadly consistent with the expected yields from Type II supernovae of low-metallicity progenitors (Woosley & Weaver 1995; Chieffi & Limongi 2004). Low- and intermediate-mass stars should not contribute significantly to the enrichment of these systems since these stars will not have had time to evolve by $z \sim 6$ (although see Barth et al. 2003). We can use the O/Si ratio to constrain the enrichment from zero-metallicity very massive stars (VMSs, $M_\star \sim 140 - 270\,M_\odot$). VMSs exploding as pair instability supernovae are expected to yield ~ 4 times as much silicon compared to Type II SNe for the same amount of oxygen (Schaerer 2002; Umeda & Nomoto 2002; Heger & Woosley 2002; Woosley & Weaver 1995; Chieffi & Limongi 2004). We can estimate the fraction $f_{\rm Si}^{\rm VMS}$ of silicon contributed by VMSs to these systems using the simple mixing scheme of Qian & Wasserburg (2005a,b),

$$\left(\frac{\rm O}{\rm Si}\right) = \left(\frac{\rm O}{\rm Si}\right)_{\rm VMS} f_{\rm Si}^{\rm VMS} + \left(\frac{\rm O}{\rm Si}\right)_{\rm SN\,II} \left(1 - f_{\rm Si}^{\rm VMS}\right). \tag{9}$$

Adopting [O/Si]$_{\rm VMS} = -0.61$ from Heger & Woosley (2002), and [O/Si]$_{\rm SN\,II} = 0.00$ from Woosley & Weaver (1995), the mean uncorrected O/Si gives $f_{\rm Si}^{\rm VMS} = 0.11 \pm 0.17$ (2σ).

However, this value of O/Si should be considered a lower limit. The ionization potential of O I is smaller than that of Si II ($\Delta E_{\text{O I}} = 13.6$ eV, $\Delta E_{\text{Si II}} = 16.3$ eV). Therefore, applying an ionization correction would increase O/Si. Taking $\langle[\text{O/Si}]\rangle > -0.10$ gives $f_{\text{Si}}^{\text{VMS}} < 0.27$ (2σ).

The mean C/Si ratio is consistent with zero silicon contribution from VMSs, although C/Si may decrease if ionization corrections are applied ($\Delta E_{\text{C II}} = 24.4$ eV $> \Delta E_{\text{Si II}}$). Dust corrections would also decrease C/Si since silicon is more readily depleted onto grains (Savage & Sembach 1996). Our upper limit of $\langle[\text{C/Si}]\rangle < -0.27$ (2σ) therefore does not provide an additional constraint on $f_{\text{Si}}^{\text{VMS}}$. However, the limit set by O/Si may still imply that VMSs provided a smaller fraction of the metals in these O I systems than in the general IGM. Qian & Wasserburg (2005a,b) have argued that VMSs at $z \gtrsim 15$ must have contributed $\gtrsim 50\%$ of the silicon in the IGM in order to produce $[\text{Si/C}]_{\text{IGM}} \sim 0.7$ at $z \approx 2-4$ (Aguirre et al. 2004). However, the Si/C ratio in the IGM derived from high-ionization lines depends sensitively on the choice of ionizing backgrounds.

The high level of absorption blueward of the Lyα emission line at $z > 5$ prevents us from reliably fitting Voigt profiles to H I. However, transmission peaks in the Lyα and Lyβ forests near the O I redshifts allow us to set upper limits on the H I column density for two of our systems. Fits to these systems with the strongest allowable damping wings are shown in Figures 7 and 8, and the corresponding limits are listed in Table 3. The limits take into account uncertainties in the continuum level, which was set to a power-law $F_\nu \propto \lambda^{-\beta}$ with spectral index $\beta = 0.5$, normalized at a rest wavelength of 1280 Å. The continuum uncertainty will include the error in the amplitude of the power law at the wavelength of the damped system. Taking $\Delta\beta = 0.65$ to incorporate 95% of the scatter in QSO spectral indices (Richards et al. 2001), this error is $< 10\%$ for the system at $z_{\text{sys}} = 5.3364$, for which the limit on $N_{\text{H I}}$ was set using Lyα transmission, and $< 20\%$ for the system at $z_{\text{sys}} = 6.0097$, for which the limit was set using Lyβ. Larger uncertainties in the continuum may result from errors in the relative flux calibration and the departure from a power law. We conservatively estimate both of these to be $\sim 20\%$, which translates to an uncertainty in the column density $\sigma(\log N_{\text{H I}}) \sim 0.3$. The upper limits on $\log N_{\text{H I}}$ listed in Table 3 are our "best fit" values plus this uncertainty. The corresponding limits on the absolute abundances are $[\text{O/H}] > -2.4$ ($z_{\text{sys}} = 5.3364$) and $[\text{O/H}] > -4.1$ ($z_{\text{sys}} = 6.0097$).

The comoving mass density for each ion is given by

$$\Omega_{\text{ion}} = \frac{H_0 m_{\text{ion}}}{c \rho_{\text{crit}}} \frac{\sum N_{\text{ion}}}{\Delta X^{\text{tot}}} , \qquad (10)$$

where m_{ion} is the mass of the ion, $\rho_{\text{crit}} = 0.92 \times 10^{-29} \, h_{70}^2$ g cm^{-3} is the cosmological closure density, and ΔX^{tot} is the total pathlength interval over which we are sensitive to O I. In Table 4 we list Ω_{ion} for O I, Si II, and C II summing over all $z_{\text{QSO}} > 4.8$ sightlines, over the

three sightlines with $z_{\mathrm{QSO}} > 6.2$ only, and over the sightline towards SDSS J1148+5251 only. The mass densities include all confirmed absorption components, including those without detected O I. However, we have made no attempt to correct for incompleteness. The densities of low-ionization metal species along our $z_{\mathrm{QSO}} > 6.2$ sightlines are comparable to the densities of the corresponding high-ionization species at lower-redshift. Songaila (2005) measured $\Omega(\mathrm{C\ IV}) \sim 3 \times 10^{-8}$ and $\Omega(\mathrm{Si\ IV}) \sim 1 \times 10^{-8}$ over $1.5 < z < 4.5$, with a drop in $\Omega(\mathrm{C\ IV})$ by at least a factor of two at $z > 5$. A decrease in high-ionization metals and a correlated rise in their low-ionization counterparts with redshift might signal a change in the ionization state of the $z > 5$ IGM. However, coverage of C IV does not currently extend to $z \sim 6$, and our O I sample is probably too small to make a meaningful comparison.

6. Discussion

Although we observe an overabundance of O I at $z > 6$ along one of our highest-redshift sightlines, it is not clear that these four systems constitute a "forest" which would signal a predominantly neutral IGM. In the reionization phase prior to the overlap of ionized bubbles, Oh (2002) predicts tens to hundreds of O I lines with $N_{\mathrm{O\ I}} > 10^{14}$ cm^{-2}, although the number may be lower if the enriched regions have very low metallicity ($Z < 10^{-2.5} Z_{\odot}$), or if the volume filling factor of metals is small ($f_Z \ll 0.01$). The number of O I systems we detect is more consistent with his predictions for the post-overlap phase, although the expected number of lines depends on the ionizing efficiency of the metal-producing galaxies. The Oh (2002) model also predicts lines with $N_{\mathrm{O\ I}} > 10^{15}$ cm^{-2}, which we do not observe.

The significance of the excess O I towards SDSS J1148+5251 is complicated by the presence of Lyα and Lyβ transmission along that sightline. The O I systems occur interspersed in redshift with the Lyβ peaks, with the velocity separation from the nearest peak ranging from $\Delta v \sim 500$ to 3000 km s^{-1} ($\Delta l \sim 5$ to 30 comoving Mpc). The O I absorbers also do not appear to be clustered. Along a total redshift interval $\Delta z_{\mathrm{tot}} = 0.49$ (~ 200 comoving Mpc) where we are sensitive to O I, the detected systems are separated by $\Delta z = 0.06$ to 0.12 ($\Delta l = 24$ to 50 comoving Mpc). If any significantly neutral regions are present along this sightline, then they occur within or near regions that are highly ionized. In contrast, we find no O I towards SDSS J1030+0524, despite the fact that its spectrum shows complete absorption in Lyα and Lyβ over $\Delta z \sim 0.2$. The SDSS J1030+0524 sightline may pass through a region of the IGM that is still largely neutral and not yet enriched. Alternatively, there may be no O I because the sightline is highly ionized. In that case, a large-scale density enhancement could still produce the high Lyα and Lyβ optical depth (Wyithe & Loeb 2005).

The overabundance of O I together with the transmission in Lyα and Lyβ indicates that

the SDSS J1148+5251 sightline has experienced both significant enrichment *and* ionization. One explanation is that we are looking along a filament. The total comoving distance between O I systems towards SDSS J1148+5251 is ≈ 101 Mpc, which is smaller than the largest known filamentary structures at low redshift (e.g., Gott et al. 2005). If the line-of-sight towards SDSS 1148+5251 runs along a filament at $z \sim 6$ then we might expect to intersect more than the average number of absorbers. Galaxies along such a structure might produce enough ionizing radiation to create the transmission gaps observed in the Lyα and Lyβ forests while still allowing pockets of neutral material to persist if the ionizing background is sufficiently low. If we assume that every $z \sim 6$ galaxy is surrounded by an enriched halo, then we can calculate the typical halo radius

$$R_{\text{halo}} \quad \sim \quad \left[\frac{\mathcal{N}}{\pi(1+z)^2 \langle \Phi_{\text{gal}} \rangle \delta_{\text{gal}} \Delta D} \right]^{1/2} \tag{11}$$

$$\sim \quad 35 \text{ proper kpc} \left(\frac{\mathcal{N}}{4} \right)^{1/2} \left(\frac{1+z}{7.2} \right)^{-1} \left(\frac{\langle \Phi_{\text{gal}} \rangle}{0.01 \, \text{Mpc}^{-3}} \right)^{-1/2}$$

$$\times \left(\frac{\delta_{\text{gal}}}{10} \right)^{-1/2} \left(\frac{\Delta D}{200 \, \text{Mpc}} \right)^{-1/2} . \tag{12}$$

Here, ΔD is the total comoving distance over which we are sensitive to O I. We have used the mean comoving number of galaxies $\langle \Phi_{\text{gal}} \rangle$ at $z \sim 6$ measured down to the limit of the Hubble Ultra Deep Field (UDF; Yan & Windhorst 2004; Bouwens et al. 2005), and assumed an overdensity of galaxies $\delta_{\text{gal}} = \Phi_{\text{gal}} / \langle \Phi_{\text{gal}} \rangle = 10$ along this sightline. The absorption could be due to filled halos, shells, or other structures surrounding the galaxies. Note that by inverting Eq. 11 we can rule out the possibility that these O I systems arise from the central star-forming regions of galaxies similar those observed in the UDF. The small size $R_{\text{half-light}} \sim 0.8$ kpc of galaxies at $z \sim 6$ (Bouwens et al. 2005) would require either a local galaxy overdensity $\delta_{\text{gal}} \sim 10^4$ or a large number of faint galaxies to produce the observed absorption systems.

At present we can place relatively few physical constraints on these absorbers. Assuming charge-exchange equilibrium (Eq. 1), we can estimate the H I column densities as a function of metallicity,

$$\log N_{\text{H I}} = 16.9 + \log \left(\frac{N_{\text{O I}}}{10^{13.7} \, \text{cm}^{-2}} \right) - [\text{O/H}] . \tag{13}$$

For solar metallicities, even the weakest O I system in our sample must be nearly optically thick. Metal-poor absorbers with $[\text{O/H}] < -2$ would require column densities $N_{\text{H I}} \gtrsim 10^{19} \, \text{cm}^{-2}$, which is consistent with the indication from the relative metal abundances that these absorbers are largely neutral.

Finally, the excess O I absorbers are distinguished by their small velocity dispersions.

Three out of the four systems towards SDSS J1148+5251 have single components with Doppler widths $b \approx 5 - 8$ km s^{-1}. We may be seeing only the low-ionization component of a kinematically more complex structure such as a galactic outflow (e.g., Simcoe et al. 2005). However, if there are additional high-ionization components that would appear in C IV and Si IV then we might expect to see components in C II and possibly Si II without O I. This is the case in the $z_{\mathrm{sys}} = 5.3364$ system towards SDSS J0231-0728. The $z_{\mathrm{sys}} = 6.1293$ and $z_{\mathrm{sys}} = 6.2550$ systems towards SDSS J1148+5251 show potential C II lines that do not appear in O I, but these are relatively weak, and in the $z_{\mathrm{sys}} = 6.1293$ system there is no apparent strong Si IV. Among the 11 O I absorbers in the $z < 4.6$ sample, only three have a single O I component with a velocity width comparable to the three narrowest systems towards SDSS J1148+5251. The fact that the excess O I systems appear kinematically quiescent further suggests that they are a distinct class of absorbers.

7. Summary

We have conducted a search for O I in the high-resolution spectra of 9 QSOs at $4.8 \leq z_{\mathrm{QSO}} \leq 6.4$. In total, we detect six systems in the redshift intervals where O I $\lambda1302$ falls redward of the Lyα forest. Four of these lie towards SDSS J1148+5251 ($z_{\mathrm{QSO}} = 6.42$). This imbalance is not easily explained by small number statics or by varying sensitivity among the data. A search at lower redshift revealed no more than than one O I system per sightline in a high-quality sample of 30 QSOs with $2.6 \leq z_{\mathrm{QSO}} \leq 4.6$. The number of excess systems is significantly larger than the expected number of damped Lyα systems at $z \sim 6$, but similar to the predicted number of Lyman limit systems.

The six systems have mean relative abundances $\langle[\mathrm{O/Si}]\rangle = -0.04 \pm 0.06$, $\langle[\mathrm{C/O}]\rangle = -0.31 \pm 0.09$, and $\langle[\mathrm{C/Si}]\rangle = -0.34 \pm 0.07$ (2σ errors), assuming no ionization corrections. These abundances are consistent with enrichment dominated by Type II supernovae. The lower limit on the oxygen to silicon ratio $\langle[\mathrm{O/Si}]\rangle > -0.10$ is insensitive to ionization corrections and limits the contribution of silicon from VMSs to $< 30\%$ in these systems. The upper limits on the ratio of carbon to oxygen $[\mathrm{C/O}] \leq -0.13$, and carbon to silicon $[\mathrm{C/Si}] \leq -0.20$ are also insensitive to ionization. Integrating over only the confirmed absorption lines, the mean ionic comoving mass densities along the three $z_{\mathrm{QSO}} > 6.2$ sightlines are $\Omega_{\mathrm{O\,I}} \approx 7.0 \times 10^{-8}$, $\Omega_{\mathrm{Si\,II}} \approx 9.6 \times 10^{-9}$, and $\Omega_{\mathrm{C\,II}} \approx 1.5 \times 10^{-8}$.

The excess O I systems towards SDSS J1148+5251 occur in redshift among Lyα and Lyβ transmission features, which indicates that the IGM along this sightline has experienced both enrichment *and* significant ionization. The sightline may pass along a filament, where galaxies are producing enough ionizing photons create the transmission gaps while still allowing a

few neutral absorbers to persist. In contrast, no O I was observed towards SDSS J1030+0524, whose spectrum shows complete Gunn-Peterson absorption. The SDSS J1030+0524 sightline may pass through an underdense region containing very few sources that would either enrich or ionize the IGM. Alternatively, the sightline may be highly ionized, with a large-scale density enhancement producing strong line-blending in the Lyα and Lyβ forests. Future deep imaging of these fields and near-infrared spectroscopy covering high-ionization metal lines will allow us to distinguish between these scenarios and clarify the nature of the excess O I absorbers.

REFERENCES

Aguirre, A., Schaye, J., Kim, T.-S., Theuns, T., Rauch, M., & Sargent, W. L. W. 2004, ApJ, 602, 38

Barth, A. J., Martini, P., Nelson, C. H., & Ho, L. C. 2003, ApJ, 594, L95

Becker, R. H., et al. 2001, AJ, 122, 2850

Bouwens, R. J., Illingworth, G. D., Blakeslee, J. P., & Frankx, M. 2005, ApJ, submitted (astro-ph/05090641)

Carilli, C. L., Gnedin, N., Furlanetto, S., & Owen, F. 2004, New Astronomy Review, 48, 1053

Chieffi, A., & Limongi, M. 2004, ApJ, 608, 405

Djorgovski, S. G., Castro, S., Stern, D., & Mahabal, A. A. 2001, ApJ, 560, L5

Fan, X., et al. 2001, AJ, 122, 2833

Fan, X., Narayanan, V. K., Strauss, M. A., White, R. L., Becker, R. H., Pentericci, L., & Rix, H.-W. 2002, AJ, 123, 1247

Fan, X., et al. 2003, AJ, 125, 1649

Fan, X., et al. 2004, AJ, 128, 515

Furlanetto, S. R., & Loeb, A. 2003, ApJ, 588, 18

Furlanetto, S. R., Hernquist, L., & Zaldarriaga, M. 2004, MNRAS, 354, 695

Furlanetto, S. R., Zaldarriaga, M., & Hernquist, L. 2004, ApJ, 613, 16

Furlanetto, S. R., & Oh, S. P. 2005, MNRAS, submitted (astro-ph/0505065)

Gott, J. R. I., Jurić, M., Schlegel, D., Hoyle, F., Vogeley, M., Tegmark, M., Bahcall, N., & Brinkmann, J. 2005, ApJ, 624, 463

Grevesse, N., & Sauval, A. J. 1998, Space Science Reviews, 85, 161

Gunn, J. E., & Peterson, B. A. 1965, ApJ, 142, 1633

Heger, A., & Woosley, S. E. 2002, ApJ, 567, 532

Horne, K. 1986, PASP, 98, 609

Kassim, N. E., Lazio, T. J. W., Ray, P. S., Crane, P. C., Hicks, B. C., Stewart, K. P., Cohen, A. S., & Lane, W. M. 2004, P&SS, 52, 1343

Kelson, D. D. 2003, PASP, 115, 688

Malhotra, S., & Rhoads, J. E. 2004, ApJL, 617, L5

Oh, S. P. 2002, MNRAS, 336, 1021

Oh, S. P., & Furlanetto, S. R. 2005, ApJ, 620, L9

Osterbrock, D. E. 1989, Astrophysics of Gaseous Nebulae and Active Galactic Nuclei (Sausalito, CA: University Science Books)

Pentericci, L., et al. 2002, AJ, 123, 2151

Péroux, C., McMahon, R. G., Storrie-Lombardi, L. J., & Irwin, M. J. 2003, MNRAS, 346, 1103

Pettini, M., Shapley, A. E., Steidel, C. C., Cuby, J.-G., Dickinson, M., Moorwood, A. F. M., Adelberger, K. L., & Giavalisco, M. 2001, ApJ, 554, 981

Press, W. H., & Schechter, P. 1974, ApJ, 187, 425

Prochaska, J. X., et al. 2001, ApJS, 137, 21

Prochaska, J. X., Gawiser, E., Wolfe, A. M., Cooke, J., & Gelino, D. 2003, ApJS, 147, 227

Prochaska, J. X., Herbert-Forte, S., & Wolfe, A. M. 2005, ApJ, submitted (astro-ph/0508361)

Qian, Y.-Z., & Wasserburg, G. J. 2005, ApJ, 623, 17

Qian, Y.-Z., & Wasserburg, G. J. 2005, ApJ, submitted (astro-ph/0509151)

Rao, S. M., Turnshek, D. A., & Nestor, B. D. 2005, ApJ, submitted (astro-ph/0509469)

Richards, G. T., et al. 2001, AJ, 121, 2308

Santos, M. R. 2004, MNRAS, 349, 1137

Savage, B. D., & Sembach, K. R. 1996, ARA&A, 34, 279

Schaerer, D. 2002, A&A, 382, 28

Schaye, J., Aguirre, A., Kim, T.-S., Theuns, T., Rauch, M., & Sargent, W. L. W. 2003, ApJ, 596, 768

Sheth, R. K., & Tormen, G. 2002, MNRAS, 329, 61

Simcoe, R. A., Sargent, W. L. W., & Rauch, M. 2004, ApJ, 606, 92

Simcoe, R. A., Sargent, L. W. L., Rauch, M., & Becker, G. D. 2005, ApJ, submitted (astro-ph/0508116)

Songaila, A. 2004, AJ, 127, 2598

Songaila, A. 2005, AJ, 130, 1996

Stern, D., Yost, S. A., Eckart, M. E., Harrison, F. A., Helfand, D. J., Djorgovski, S. G., Malhotra, S., & Rhoads, J. E. 2005, ApJ, 619, 12

Storrie-Lombardi, L. J., & Wolfe, A. M. 2000, ApJ, 543, 552

Tozzi, P., Madau, P., Meiksin, A., & Rees, M. J. 2000, ApJ, 528, 597

Umeda, H., & Nomoto, K. 2002, ApJ, 565, 385

Vogt, S. S., et al. 1994, Proc. SPIE, 2198, 362

White, R. L., Becker, R. H., Fan, X., & Strauss, M. A. 2003, AJ, 126, 1

White, R. L., Becker, R. H., Fan, X., & Strauss, M. A. 2005, AJ, 129, 2102

Woosley, S. E., & Weaver, T. A. 1995, ApJS, 101, 181

Wyithe, S., & Loeb, A. 2005, ApJ, submitted (astro-ph/0508604)

Yan, H., & Windhorst, R. A. 2004, ApJ, 612, L93

Table 1.   Summary of Observations

QSO	z_{QSO}	Dates	Δt_{exp} (hrs)[a]
SDSS J2225−0014	4.87	2004 Jun	6.7[b]
SDSS J1204−0021	5.09	2005 Jan - Feb	6.7
SDSS J0915+4244	5.20	2005 Jan - Feb	10.8
SDSS J0231−0728	5.42	2005 Jan - Feb	10.0
SDSS J0836+0054	5.80	2003 Feb - 2005 Jan	21.7[c]
SDSS J0002+2550	5.82	2005 Jan - Jun	4.2
SDSS J1623+3112	6.22	2005 Jun	12.5
SDSS J1030+0524	6.30	2005 Feb	12.0
SDSS J1148+5251	6.42	2003 Feb - 2005 Feb	22.0[d]

[a]All exposures were taken with the upgraded HIRES detector unless otherwise noted.

[b]Taken with the old HIRES detector

[c]9.2 hrs taken with the old HIRES detector

[d]4.2 hrs taken with the old HIRES detector

Table 2.   Measured Properties of O I Systems

Ion	z	b (km s^{-1})	$\log N$ (cm^{-2})
	SDSS J0231−0728: $z_{\rm sys} = 5.3364$		
Si II	5.333982 ± 0.000008	5.38 ± 0.58	12.786 ± 0.055
C II[a]	5.333982	5.38	13.584 ± 0.068
Si II	5.335928 ± 0.000020	6.91 ± 1.33	12.514 ± 0.079
Si II	5.336337 ± 0.000019	7.62 ± 1.60	12.978 ± 0.087
Si II[b]	5.336721	12.96	12.711 ± 0.135
O I[a]	5.335928	6.91	13.982 ± 0.086
O I[a]	5.336337	7.62	14.138 ± 0.129
O I	5.336721 ± 0.000072	12.96 ± 3.23	13.972 ± 0.143
C II[a]	5.335928	6.91	13.298 ± 0.077
C II[a]	5.336337	7.62	13.454 ± 0.119
C II[b]	5.336721	12.96	13.314 ± 0.138
Si II	5.337841 ± 0.000014	10.89 ± 0.98	12.678 ± 0.040
Si II	5.338474 ± 0.000043	11.71 ± 3.39	12.233 ± 0.098
Si II	5.339301 ± 0.000016	10.44 ± 1.13	12.316 ± 0.063
C II[a]	5.337841	10.89	13.512 ± 0.051
C II[a]	5.338474	11.71	12.880 ± 0.161
C II[a]	5.339301	10.45	13.074 ± 0.097
Si IV[a]	5.337841	10.89	12.848 ± 0.051
Si IV[a]	5.338474	11.71	12.142 ± 0.192
Si IV[a]	5.339301	10.44	12.950 ± 0.049
	SDSS J1623+3112: $z_{\rm sys} = 5.8408$		
O I[c]	5.836481 ± 0.000012	5.01 ± 0.59	14.376 ± 0.075
O I[c]	5.836806 ± 0.000017	4.44 ± 1.57	14.216 ± 0.111
Si II[c]	5.836423 ± 0.000029	3.63 ± 2.66	12.746 ± 0.182
Si II[c]	5.836799 ± 0.000060	10.82 ± 4.29	12.985 ± 0.124
Si II[d]	5.839938	6.37	13.279 ± 0.182
Si II[d]	5.840138	4.13	13.063 ± 0.340
Si II[b]	5.840456	6.92	12.931 ± 0.196
Si II[b]	5.840798	5.32	13.488 ± 0.060
Si II[b]	5.841113	7.33	13.271 ± 0.078
Si II[b]	5.841456	1.77	11.655 ± 1.018
Si II[d]	5.841780	6.23	12.854 ± 0.070
O I[d]	5.839938	6.37	14.214 ± 0.212
O I[d]	5.840138	4.13	14.152 ± 0.242
O I	5.840456 ± 0.000032	6.92 ± 4.21	13.734 ± 0.206
O I	5.840798 ± 0.000014	5.32 ± 0.94	14.384 ± 0.084
O I	5.841113 ± 0.000025	7.33 ± 1.48	14.316 ± 0.073
O I	5.841456 ± 0.000014	1.77 ± 1.72	13.518 ± 0.150
O I[d]	5.841780	6.23	13.793 ± 0.027
C II	5.839938 ± 0.000055	6.37 ± 1.56	13.811 ± 0.231
C II	5.840138 ± 0.000039	4.13 ± 2.50	13.955 ± 0.249

Table 2—Continued

Ion	z	b (km s^{-1})	$\log N$ (cm^{-2})
C II[b]	5.840456	6.92	13.431 ± 0.193
C II[b]	5.840798	5.32	13.771 ± 0.093
C II[b]	5.841113	7.33	13.316 ± 0.101
C II	5.841780 ± 0.000007	6.23 ± 0.51	13.736 ± 0.055
SDSS J1148+5251: $z_{\mathrm{sys}} = 6.0097$			
Si II[b]	6.009119	7.02	12.126 ± 0.592
Si II[b]	6.009290	3.36	12.770 ± 0.137
Si II[b]	6.009717	8.44	13.323 ± 0.037
Si II[b]	6.010070	4.94	12.331 ± 0.261
O I	6.009119 ± 0.000112	7.02 ± 3.18	13.593 ± 0.371
O I	6.009290 ± 0.000012	3.36 ± 1.28	14.071 ± 0.113
O I	6.009717 ± 0.000010	8.44 ± 0.96	14.487 ± 0.030
O I	6.010070 ± 0.000034	4.94 ± 1.60	13.516 ± 0.178
C II[b]	6.009119	7.02	13.180 ± 0.328
C II[b]	6.009290	3.36	13.281 ± 0.286
C II[b]	6.009717	8.44	14.013 ± 0.057
C II[b]	6.010070	4.94	13.044 ± 0.182
SDSS J1148+5251: $z_{\mathrm{sys}} = 6.1293$			
C II[c]	6.127673 ± 0.000039	6.11 ± 3.03	12.916 ± 0.118
C II[c]	6.128589 ± 0.000037	8.08 ± 2.47	13.101 ± 0.092
Si II[b]	6.129267	6.51	13.273 ± 0.050
O I	6.129267 ± 0.000006	6.51 ± 0.49	14.606 ± 0.096
C II[b]	6.129267	6.51	13.744 ± 0.070
C II[c]	6.129885 ± 0.000017	2.21 ± 1.80	13.161 ± 0.186
SDSS J1148+5251: $z_{\mathrm{sys}} = 6.1968$			
Si II	6.196787 ± 0.000014	7.82 ± 0.84	12.277 ± 0.044
O I[a]	6.196787	7.82	13.727 ± 0.061
C II[a]	6.196787	7.82	13.027 ± 0.072
SDSS J1148+5251: $z_{\mathrm{sys}} = 6.2555$			
C II[c]	6.255234 ± 0.000131	12.13 ± 5.51	13.159 ± 0.229
Si II	6.255496 ± 0.000004	4.30 ± 0.27	12.900 ± 0.040
O I	6.255465 ± 0.000015	5.08 ± 1.04	14.075 ± 0.087
C II[a]	6.255496	4.30	13.596 ± 0.114

[a]The z- and b-values for this component were tied to those for Si II.

[b]The z- and b-values for this component were tied to those for O I.

[c]Unconfirmed component

[d]The z- and b-values for this component were tied to those for C II.

Table 3.   Abundance Measurements

Sightline	$z_{\rm sys}$	$\log N_{\rm O\,I}^{\rm tot\,a}$	$\log N_{\rm Si\,II}^{\rm tot\,a}$	$\log N_{\rm C\,II}^{\rm tot\,a}$	[O/Si][b]	[C/O][b]	[C/Si][b]	$\log N_{\rm H\,I}$
SDSS J1148+5251	6.2555	14.08 ± 0.09	12.90 ± 0.04	13.60 ± 0.11	-0.11 ± 0.08	-0.17 ± 0.15	-0.27 ± 0.12	$\cdots$
SDSS J1148+5251	6.1968	13.73 ± 0.06	12.28 ± 0.04	13.03 ± 0.07	0.17 ± 0.07	-0.39 ± 0.10	-0.22 ± 0.08	$\cdots$
SDSS J1148+5251	6.1293	14.61 ± 0.10	13.27 ± 0.05	13.74 ± 0.07	0.05 ± 0.10	-0.55 ± 0.13	-0.50 ± 0.09	$\cdots$
SDSS J1148+5251	6.0097	14.70 ± 0.05	13.48 ± 0.05	14.17 ± 0.07	-0.07 ± 0.06	-0.22 ± 0.09	-0.28 ± 0.08	< 21.9[c]
SDSS J1623+3112	5.8408	14.96 ± 0.06	13.98 ± 0.06	14.50 ± 0.09	-0.31 ± 0.09	-0.15 ± 0.13	-0.45 ± 0.11	$\cdots$
SDSS J0231$-$0728	5.3364	14.52 ± 0.07	13.25 ± 0.06	13.84 ± 0.07	-0.02 ± 0.07	-0.37 ± 0.12	-0.39 ± 0.09	< 20.1[c]

[a]Total ionic column densities summed over all components with confirmed O I absorption

[b]Relative abundances using the solar values of Grevesse & Sauval (1998) and assuming no ionization corrections

[c]Upper limit including uncertainty in the continuum level

Table 4.   Comoving Mass Densities[a]

Sightlines	$\Omega(\text{O I})$ $(\times 10^{-8})$	$\Omega(\text{Si II})$ $(\times 10^{-9})$	$\Omega(\text{C II})$ $(\times 10^{-8})$
All	3.2 ± 0.2	4.5 ± 0.4	0.8 ± 0.1
$z_{\text{QSO}} > 6.2$	7.0 ± 0.6	9.6 ± 0.9	1.5 ± 0.2
SDSS J1148+5251	10.2 ± 1.0	9.8 ± 0.7	1.8 ± 0.2

[a]For each ion, the value of Ω_{ion} computed from Eq. 10 includes all *confirmed* components listed in Table 2 along the indicated lines of sight, including those components without corresponding O I. These values are lower limits in the sense that we have made no attempt to correct for incompleteness. Errors are 1σ and reflect only the uncertainty in the summed column densities.
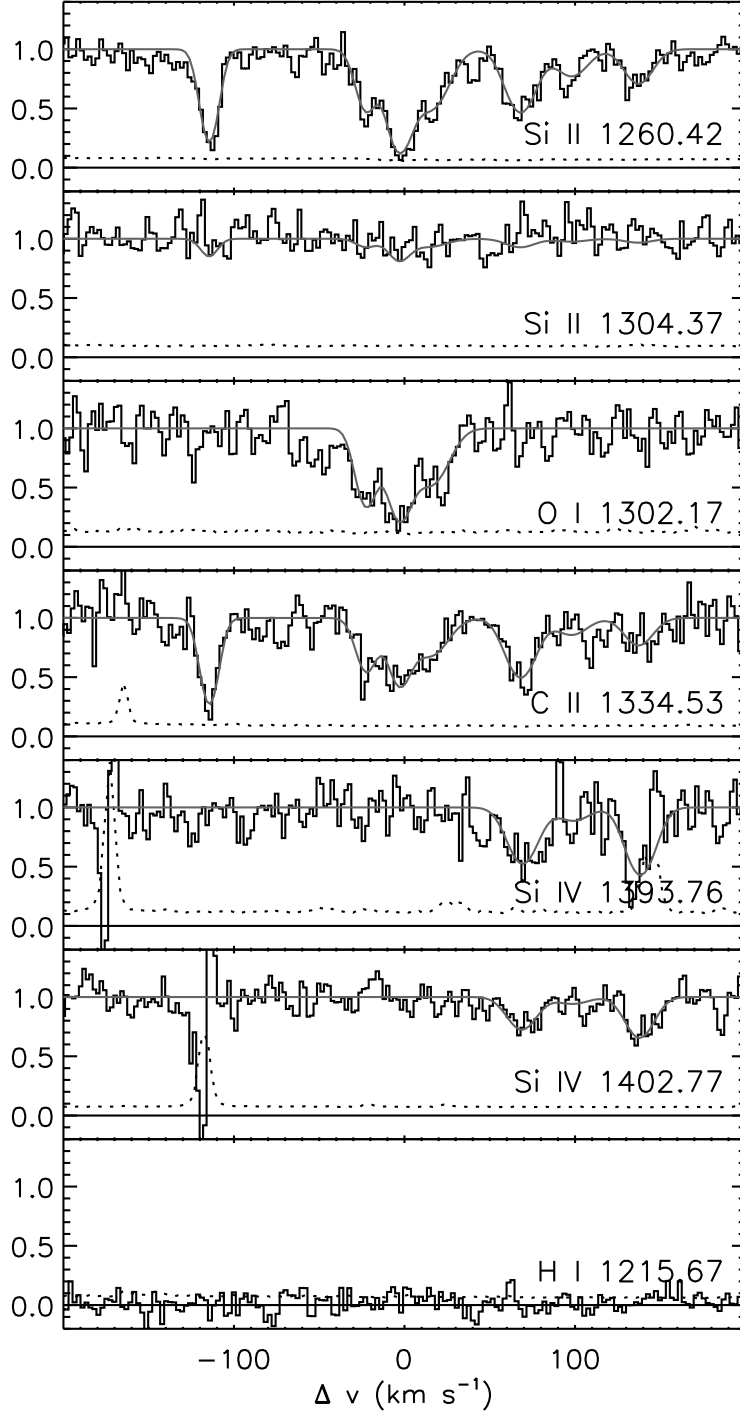
Fig. 1.— Absorption lines for the $z_{\rm sys} = 5.3364$ O I system towards SDSS J0231−0728. Regions of the spectrum covering individual transitions have been shifted onto a common velocity scale. The *histogram* shows the normalized flux. The *solid line* shows the best Voigt profile fit. The *dotted line* shows the 1σ flux error.
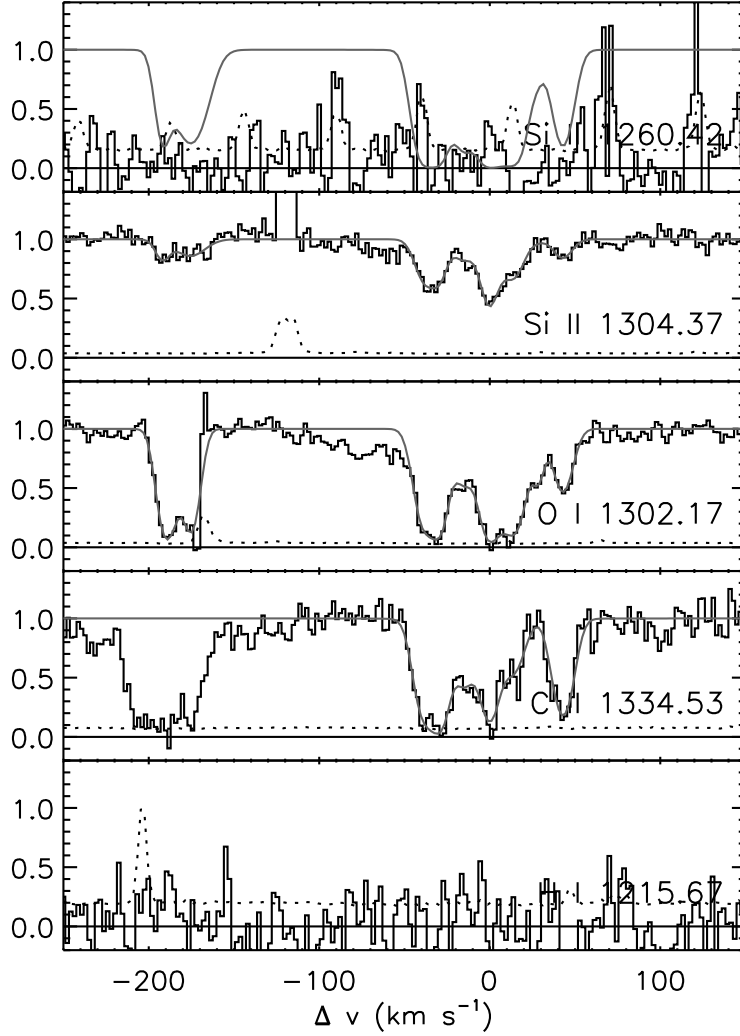
Fig. 2.— Absorption lines for the $z_{\rm sys} = 5.8408$ O I system towards SDSS 1623+3112. See Figure 1 for details. The sharp features around Si II $\lambda 1260$ are noise in the Lyα forest. The components at $\Delta v \approx -180$ km s^{-1} are unconfirmed due to the strong $z_{\rm abs} = 2.1979$ Mg I absorption at the wavelength where we would expect to see C II.
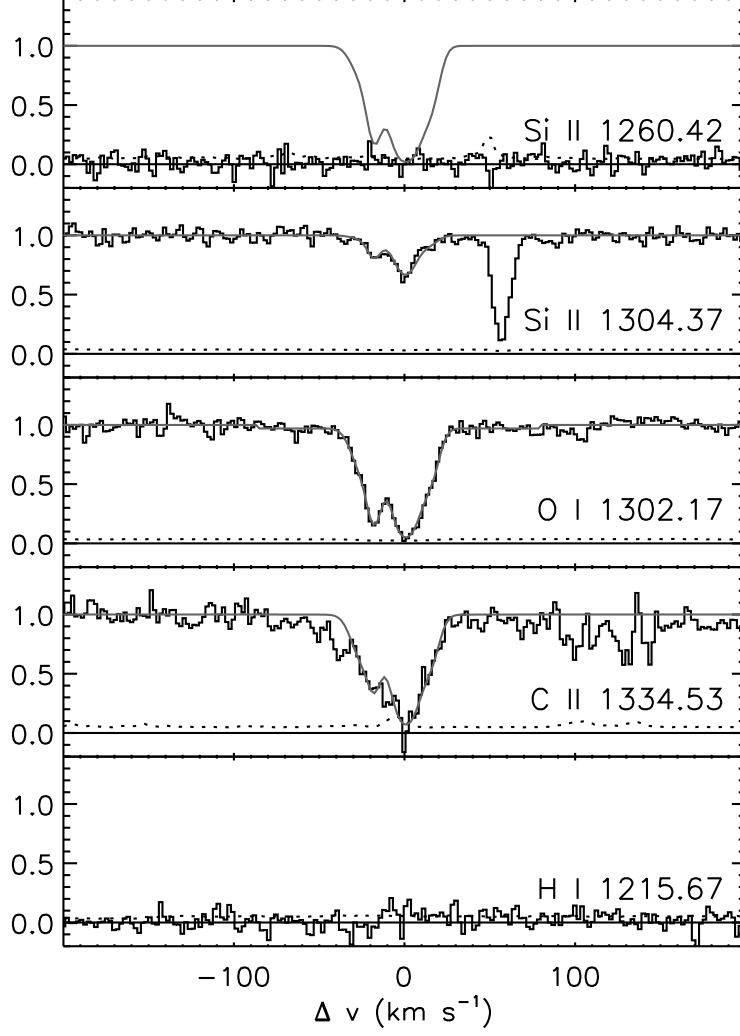
Fig. 3.— Absorption lines for the $z_{\rm sys} = 6.0097$ O I system towards SDSS 1148+5251. See Figure 1 for details. Si II $\lambda1260$ falls in the Lyα forest. The strong line at $\Delta v = 57$ km s^{-1} from Si II $\lambda1304$ is Si II $\lambda1260$ at $z = 6.2555$. The absorption features at $\Delta v \approx -40$ km s^{-1} and $\Delta v \approx 90 - 140$ km s^{-1} from C II are probably telluric absorption that has not been fully removed.
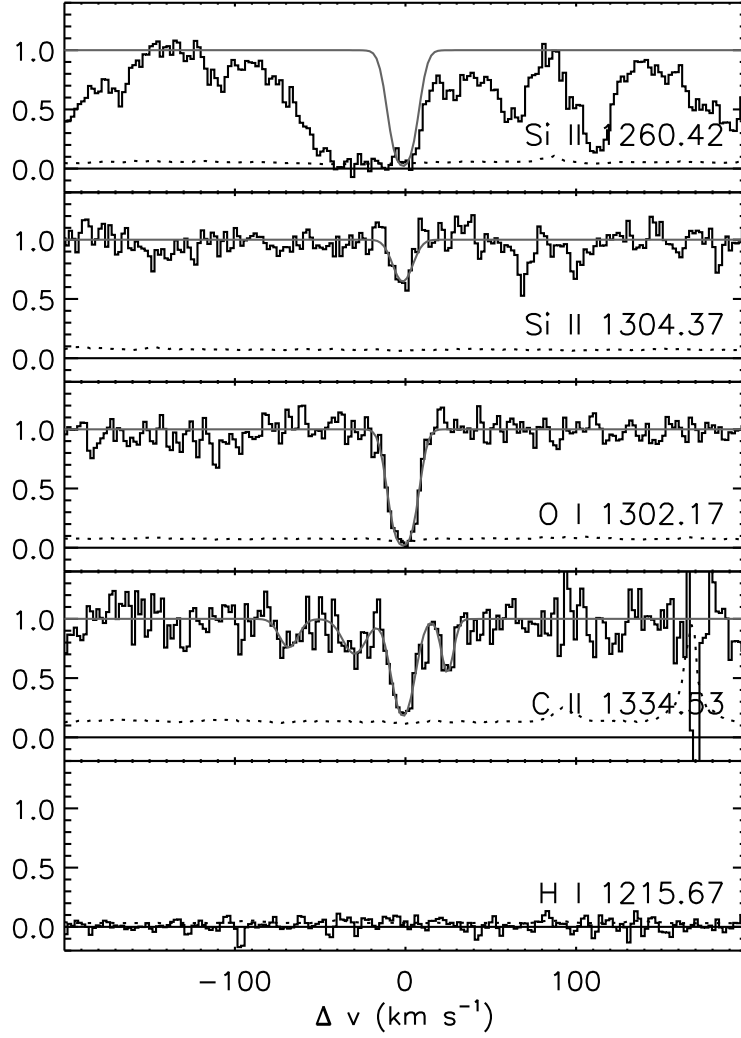
Fig. 4.— Absorption lines for the $z_{\mathrm{sys}} = 6.1293$ O I system towards SDSS 1148+5251. See Figure 1 for details. The features around Si II $\lambda 1260$ are Lyα absorption in the quasar proximity region. The C II components at $\Delta v = -67, -29$ and 26 km s^{-1} are unconfirmed.
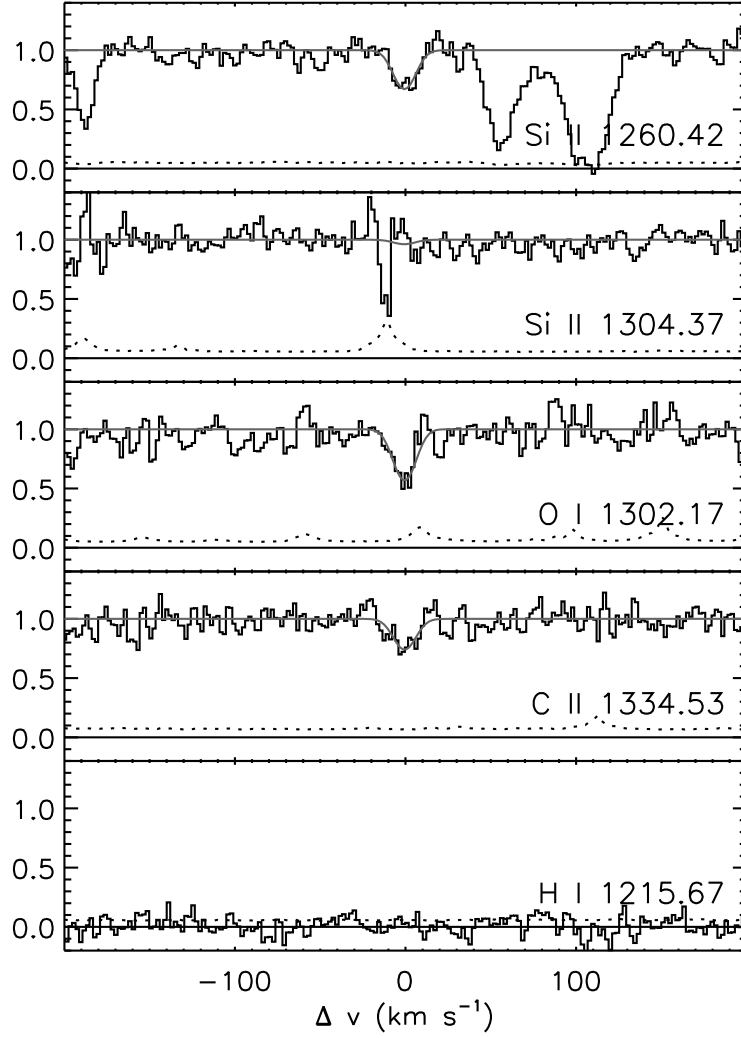
Fig. 5.— Absorption lines for the $z_{sys} = 6.1968$ O I system towards SDSS 1148+5251. See Figure 1 for details. The features near Si II $\lambda1260$ are unrelated metal lines. The sharp feature near Si II $\lambda1304$ is the residual from a strong skyline.
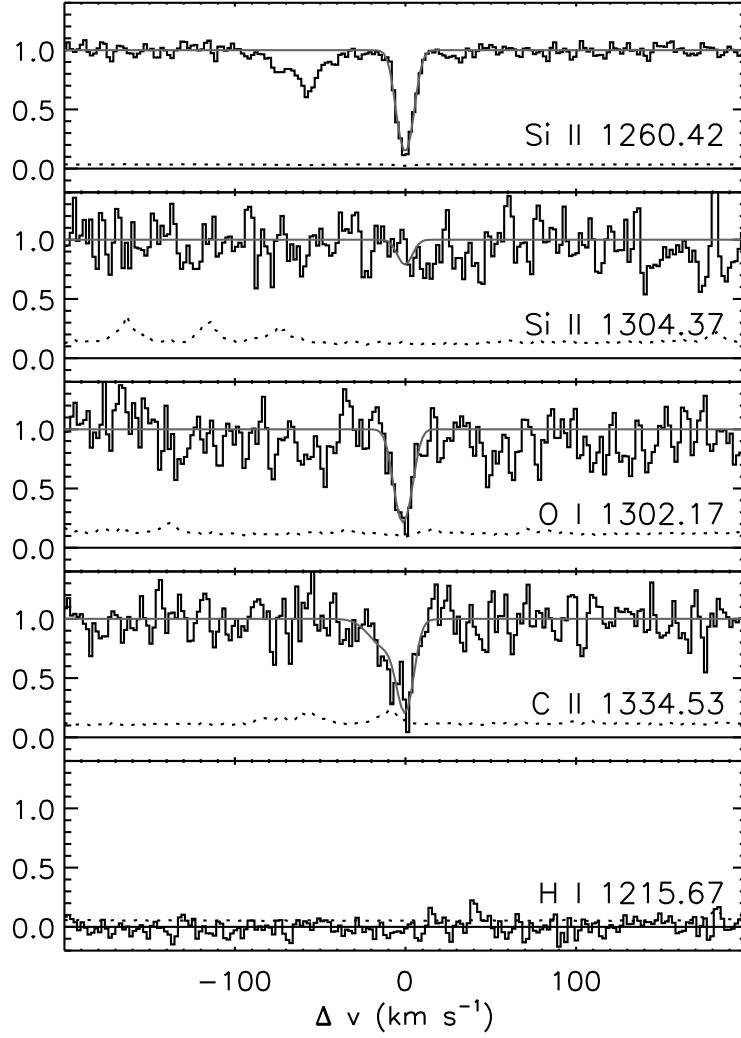
Fig. 6.— Absorption lines for the $z_{\rm sys} = 6.2555$ O I system towards SDSS 1148+5251. See Figure 1 for details. The absorption at $\Delta v \approx -60$ km s^{-1} from Si II $\lambda 1260$ is Si II $\lambda 1304$ at $z = 6.0097$. The C II fit includes an unconfirmed component on the blue edge of the profile.
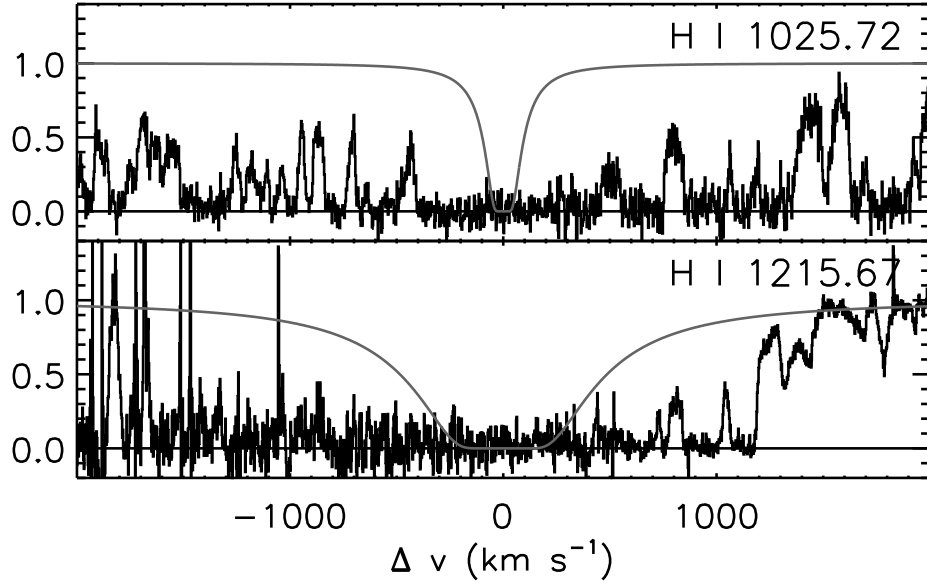
Fig. 7.— Voigt profile fit to H I Lyα and Lyβ corresponding to the upper limit on $N_{\mathrm{H\,I}}$ for the $z_{\mathrm{sys}} = 5.3364$ O I systems towards SDSS J0231−0728. In order to set an upper limit on $N_{\mathrm{H\,I}}$ we have taken $b = 1$ km s^{-1}, although the actual b-parameter is likely to be significantly larger. In this system, $N_{\mathrm{H\,I}}$ is constrained by the transmitted flux in the wings of the Lyα profile.
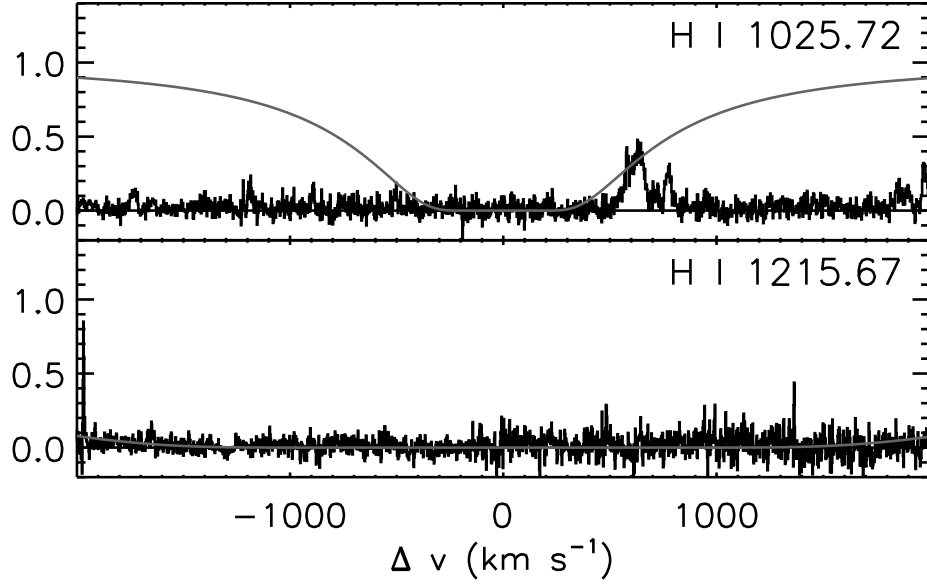
Fig. 8.— Voigt profile fit to H I Lyα and Lyβ corresponding to the upper limit on $N_{\rm H\,I}$ for the $z_{\rm sys} = 6.0097$ O I systems towards SDSS J1148+5251. In this system, $N_{\rm H\,I}$ is constrained by the transmitted flux in the red wing of the Lyβ profile.
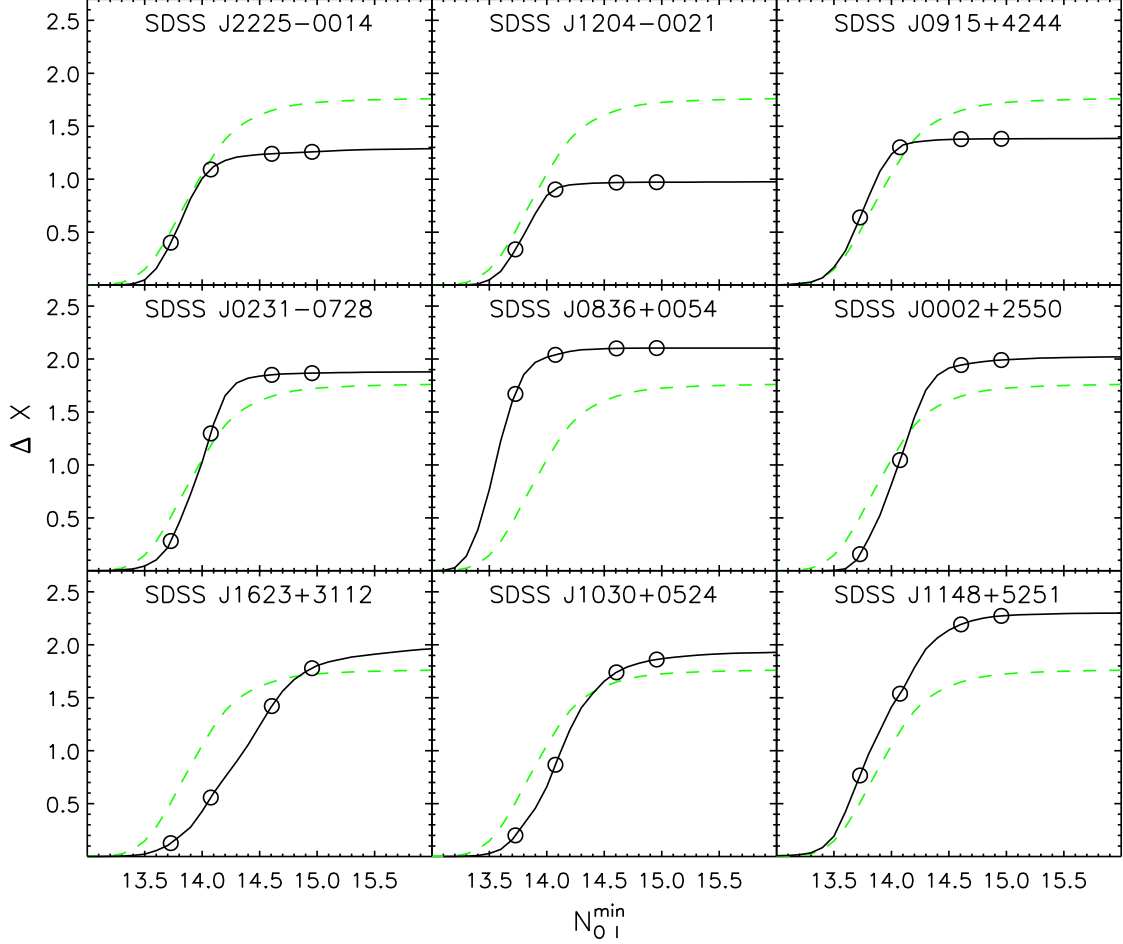
Fig. 9.— Sensitivity curves for each of our sightlines. The *solid lines* give the absorption pathlength interval over which we are sensitive to single-component O I systems with $N_{\mathrm{O\,I}} \geq N_{\mathrm{O\,I}}^{\min}$ and relative abundances similar to those of the O I systems in our sample. *Circles* mark the ΔX values corresponding to the $N_{\mathrm{O\,I}}$ of systems detected towards SDSS 1148+5251. The *dashed line* shows the mean ΔX as a function of $N_{\mathrm{O\,I}}^{\min}$ for all nine sightlines. The three lowest-redshift sightlines have smaller maximum ΔX values due in part to A-band atmospheric absorption.
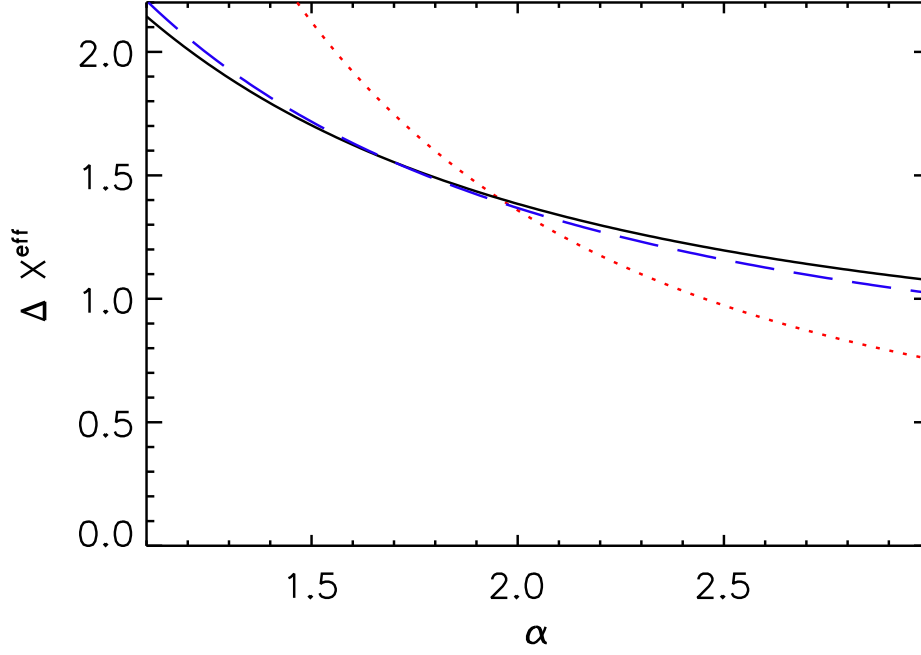
Fig. 10.— Effective absorption pathlength interval over which we are sensitive to O I systems with $N_{\rm O\,I} \geq 10^{13.7}$ cm^{-2} as a function of α, where $f(N_{\rm O\,I}) \propto N_{\rm O\,I}^{-\alpha}$ (see Eq. 3). The *solid line* shows $\Delta X^{\rm eff}$ for SDSS J1148+5251. The *dashed line* shows the summed $\Delta X^{\rm eff}$ for the remaining eight sightlines, divided by 5.7 to match SDSS J1148+5251 at $\alpha = 1.7$. The *dotted line* shows the combined $\Delta X^{\rm eff}$ for SDSS 1030+0524 and SDSS J1623+3112. For reasonable values of α, the ratio of $\Delta X^{\rm eff}$ for SDSS J1148+5251 and the remaining eight sightlines is essentially constant. We would therefore expect to see roughly six times as many O I systems along the other eight sightlines as towards SDSS J1148+5251 for a non-evolving population of absorbers.
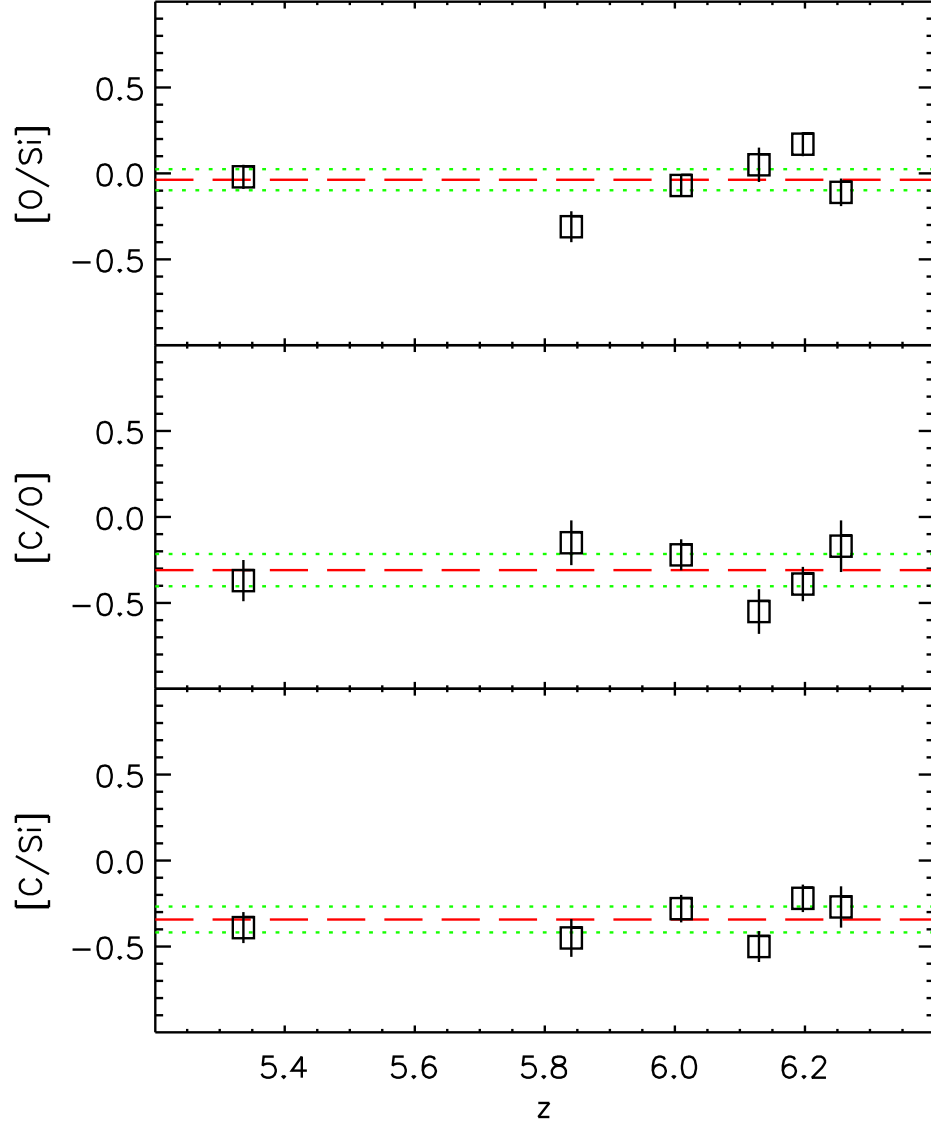
Fig. 11.— Relative metal abundances in the O I systems assuming no ionization corrections. Individual measurements plotted as *squares* with 1σ error bars are taken from Table 3. *Dashed lines* show the weighted mean values for all six systems. *Dotted lines* show the 2σ uncertainties in the means.